The effect of sodium hydroxide on Al uptake by calcium silicate hydrates (C—S—H)

Sonya Barzgar [a,b,*], Barbara Lothenbach [a,c], Mohamed Tarik [d], Alessio Di Giacomo [a,1], Christian Ludwig [b,d]
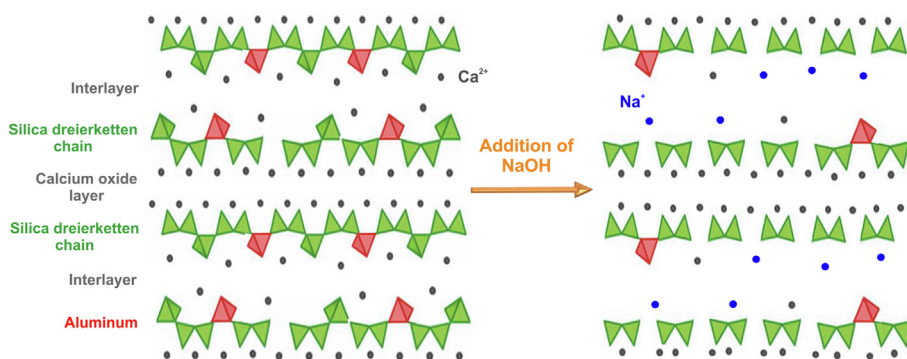
[a] Empa, Laboratory for Concrete / Construction Chemistry, CH-8610 Dübendorf, Switzerland
[b] École Polytechnique Fédéral de Lausanne (EPFL), ENAC IIE GR-LUD, CH-1015 Lausanne, Switzerland
[c] NTNU, Department of Structural Engineering, Trondheim, Norway
[d] Paul Scherrer Institute (PSI), ENE LBK CPM, 5232 Villigen PSI, Switzerland

GRAPHICAL ABSTRACT

ARTICLE INFO

ABSTRACT

To reduce the CO_2 emissions from cement production, Portland cement (PC) is partially replaced by supplementary cementitious materials (SCM). Reactions of SCM with PC during hydration leads to the formation of C—S—H with more silicon and aluminum than in PC, which affects the stability and durability of such concrete. Therefore, it is crucial to determine the role of aluminum on C—S—H properties to predict the formed hydrate phase assemblages and their effects on durability.

Aluminum sorption isotherms including very low Al concentrations have been determined for C—S—H with Ca/Si ratios from 0.6 to 1.4. Elemental measurements were performed with ICP-MS and ICP-OES. The presence of secondary phases was investigated by using thermogravimetric analysis and XRD.

Higher dissolved concentrations of Al were observed at increased alkali hydroxide concentrations and thus higher pH values. High alkali hydroxide led to an increased $Al(OH)_4^-$ formation, which reduced the Al uptake in C—S—H. This comparable behavior of Al and Si towards changes in pH values, points toward the uptake of aluminum within the silica chain both at low and high Ca/Si ratios. A higher Al uptake in C—S—H was observed at higher Ca/Si ratios, which indicates a stabilizing effect of calcium in the interlayer on Al uptake.

* Corresponding author at: Empa, Lab 308, Überland Str. 129, 8600 Dübendorf, Switzerland.
   E-mail addresses: sonya.barzgar@empa.ch (S. Barzgar), Barbara.lothenbach@empa.ch (B. Lothenbach), Mohamed.tarik@psi.ch (M. Tarik), Alessio.digiacomo@ugent.be (A. Di Giacomo), Christian.ludwig@psi.ch (C. Ludwig).
   [1] Ghent University, Department of Chemistry, Krijgslaan 281, S3, 9000 Gent, Belgium.

1. Introduction

Concrete is one of the world's most affordable, reliable, durable and readily available construction materials and is the second most consumed material after water [1]. The worldwide demand for cement production is increasing continuously and Portland cement (PC) clinker production recently is exceeding 4 billion tons annually [2]. This massive scale of production results in ~8% of the global CO_2 emissions due to its high kiln temperature and decomposition of limestone ($CaCO_3$) in raw materials [1,3–5]. About 40% of CO_2 emissions of cement production come from the combustion of fuels while approximately 60% result from the transformation of limestone into calcium oxide ($CaCO_3 \rightarrow CaO + CO_2$) [6]. Decomposition of limestone is an inevitable part of the process of manufacturing PC clinker that results in the production of approximately 0.5 tonne of CO_2 per tonne of clinker produced [6]. Reducing these CO_2 emissions is currently one of the most important and urgent research topics within the cement community [5,7]. To reduce the CO_2 footprint of PC, the clinker content of cement has to be reduced [6]. Therefore, Portland cement can be replaced partially with limestone or supplementary cementitious materials (SCM) such as blast furnace slags, by-products from steel production, fly ash from coal combustion, or calcined clays [6,8,9]. The reaction of Portland cement with different SCM, which have different chemical compositions leads to changes in the amount and composition of the hydrates [8]. This is relevant for the stability of construction materials as well as for oil well cement, such as stabilized filter ashes [10,11]. The most important hydrate formed during the reaction of Portland cement is calcium silicate hydrate (C—S—H) [7,8]. In the presence of SCM, C—S—H can have different compositions compared to the C—S—H in Portland cements. The Ca/Si molar ratio of the C—S—H present in Portland cement is in the range of 1.5–1.9 [12,13], however, in SCM blends it is in the range of 0.6 – 1.9 [14–16]. The high amount of silica in SCM such as fly ash or silica fume lowers the Ca/Si ratio of C—S—H and modifies the structure of C—S—H phases. These low Ca/Si C—S—H phases are able to take up more alkalis, but less chloride and sulfates [17,18].

If aluminum is present in the solution, C—S—H is able to incorporate aluminum [19,20] resulting in what is generally named as C—A—S—H. The C—A—S—H structure consists of calcium oxide polyhedra sheets flanked with "dreierketten" – tetrahedral (alumino) silicate chains – on both sides and counter-ions (e.g., Ca^{2+} and OH^-) and water in an interlayer on the other side [21–23]. At Ca/Si in range of 0.6–0.8, long silicate tetrahedral chains occur, in which repeating units of one bridging site is connected to two paired silicate tetrahedral sites on either side. At Ca/Si ratios above 1.0, the silica tetrahedral chains are shorter and more vacancies in the bridging sites of the silica chains occur [23–25].

The incorporation of Al as tetrahedral AlO_4 occurs into the bridging sites of silica tetrahedral chains. The presence of five-fold coordinated aluminum (Al^V) and six-fold coordinated Al (Al^{VI}) in C—A—S—H have also been described [23,26–28]. Four-fold coordinated Al^{IV} is the dominant environment in C—S—H at low Ca/Si ratios; there aluminum substitutes silicon in bridging tetrahedra of the dreierketten chain [29]. Al^{IV} has been reported to be in the bridging sites either without charge balance or are charge balanced by interlayer Ca^{2+}, Na^+, or H^+ [27]. At Ca/Si ratios above 1.0, a second Al^{IV} species is present, which has been assigned to aluminum in bridging position charge-balanced by calcium cations [26,27,30,31]. Increasing the Ca/Si ratio decreases the fraction of Al^{IV} and Al^{VI} species become dominant [26,31].

The effect of aluminum on the structure of C—S—H and their impact on hydration is still not completely understood. The comparison of the few available datasets where the uptake of aluminum by C—S—H has been measured experimentally [13,20,31–33] showed a strong dependency of the Al uptake in C—S—H on the aqueous Al concentrations. In addition, at high concentrations of Al the precipitation of katoite ($3CaO.Al_2O_3\cdot6H_2O$) and strätlingite ($2CaO.Al_2O_3\cdot SiO_2\cdot8H_2O$) occurs [32,34] which limits the Al concentration in solution and thus the Al uptake by C—S—H. The data available, however, revealed also a dependency of aluminum uptake on the reaction time and/or synthesis method used [13,17,31–33].

In most available studies, the concentrations have been measured by ion chromatography with a relatively high limit of detection of 0.004 mM Al, which is only slightly below the aluminum concentrations of 0.01 to 0.05 mM, where strätlingite and microcrystalline aluminum hydroxide start to precipitate [32]. Thus, very little is known on the effect of aluminum concentrations on the different binding sites in the C—S—H structure, and on how the different aluminum binding sites influence each other [17]. For the further development of thermodynamic models for C—S—H containing aluminum, a more comprehensive knowledge about the sorption at varying aluminum concentrations is needed.

The main aim of this study is to investigate the effect of different aluminum concentrations, different pH values and sodium hydroxide (NaOH) concentrations on the aluminum uptake in the C—S—H. The experiments were performed by synthesizing the C—S—H samples containing different Al/Si ratios, Ca/Si ratios and alkali hydroxide contents. The samples were filtrated after 3 months equilibration. Inductively coupled plasma mass spectrometry (ICP-MS) and inductively coupled plasma optical emission spectrometry (ICP-OES) were used to determine very low dissolved aluminum concentrations. The detection limit for Al in ICP-OES and ICP-MS was 4×10^{-5} mM.

Furthermore, the effect of Ca/Si ratio on the Al uptake in C—S—H was studied. The solid samples were analyzed with thermogravimetric analysis (TGA) and X-ray diffraction (XRD) to check for the presence of secondary phases in the solid phase. Moreover, the measured concentrations were compared with the calculated solubility of C—S—H using the Gibbs free energy minimization program *GEM*-Selektor [35,36].

2. Materials and methods

All synthesis were done following a one-step protocol in which a total 3.8 g of calcium oxide (CaO), silica fume (SiO_2) and calcium aluminate (CA: $CaO\cdot Al_2O_3$) were added into 171 mL of Milli-Q water or NaOH solutions (liquid/solid = 45) to obtain C—A—S—H with different compositions. CaO with 96% purity was obtained by burning calcium carbonate ($CaCO_3$, Merck, pro analysis) at 1000 °C for 12 h. SiO_2 was provided by Aerosil 200, Evonik. CA was synthesized from $CaCO_3$ and Al_2O_3 (Sigma Aldrich). The mixture was heated at 800 °C for 1 h, at 1000 °C for 4 h and at 1400 °C for 8 h. Then it is cooled down a with a rate of 600 °C/h. The proportions of CaO, SiO_2 and CA were varied to obtain C—A—S—H with different Ca/Si and Al/Si ratios as indicated in Table 1. 0.5 M NaOH corresponds to the pH value generally observed in the pore solution of cement [37,38]. In addition, NaOH concentrations of 0, 0.1 and 1 M were selected to cover the different range of pH values relevant for hydrated cements and in order to investigate the effect of pH values on Al uptake in C—S—H [13]. CASH samples were prepared at Ca/Si molar ratios between 0.6 and 1.4 and Al/Si molar ratios were varied from 0 to 0.1 with 4 different NaOH concentrations of 0, 0.1, 0.5 and 1 M. All experimental details on samples are compiled in appendix A.

All samples were synthesized in a nitrogen filled glovebox to minimize carbonation and were stored in 200 mL PE-HD containers placed on a horizontal shaker moving at 100 rpm and equilibrated at 20 °C. After 3 months, the solid and liquid phases were

Table 1
Ca/Si, Al/Si molar ratios and alkali concentrations used to prepare C—A—S—H at 20 °C.

Ca/Si	Al/Si	NaOH (mol/L)
0.6, 0.8, 1.0, 1.2 and 1.4	0 0.001 0.003 0.01 0.03 0.05 0.1	0, 0.1, 0.5 and 1

separated by vacuum filtration using nylon filters (pore size: 0.45 μm) and analyzed.

2.1. Solution phase analysis

The elemental concentrations of Na, Ca, Si and Al in the filtrates were determined with ICP-MS and ICP-OES. The different liquid samples were first acidified to 1% HNO_3 (using Suprapur HNO_3, Merck). Then, they were diluted using 1% HNO_3 to have Na concentrations below 230 mg/L and 1500 mg/L for the ICP-MS and ICP-OES analysis, respectively. Using this dilution the maximum Si and Ca concentrations were below 1 mg/L in ICP-MS. Multistandard solutions and blank solution (1% HNO_3), containing Al, Ca and Si, were prepared in the range from 0 to 200 μg/L and from 0 to 10 mg/L for ICP-MS and ICP-OES, respectively. The measurements were carried out on ICP-MS (7700x, Agilent) and/or ICP-OES (Spectro Arcos). The operating parameters used are listed in appendix C. For ICP-MS analysis [45]Sc was used to monitor the plasma stability during the analysis. More details about ICP-MS and ICP-OES measurements can be found in appendix C.

To measure the hydroxide concentration, pH measurements were made at room temperature with a Knick pH meter (pH-Meter 766) equipped with a Knick SE100 electrode. To minimize the alkali error, the pH electrode was calibrated against NaOH solutions of known concentrations.

2.2. Solid phase analysis

After filtrating the samples inside the glove box, the solids were washed first with a 50%-50% (volumetric) water–ethanol solution to avoid the precipitation of alkali during drying, and then with pure ethanol in order to remove the free water. The samples were freeze-dried during one week and then stored until analysis in nitrogen filled desiccators in the presence of saturated $CaCl_2 \cdot 2H_2O$ solution following the procedure developed by [33]. The presence or not of secondary phases in solid samples was investigated by using TGA and XRD.

TGA data were acquired with a TGA/SDTA851e Mettler Toledo device using approximately 30 mg of sample. The weight loss of the samples was recorded from 30 °C up to 980 °C with a heating rate of 20 °C/min under N_2 atmosphere. The weight losses were assigned according to the reference measurements compiled in, where the same device was used. The amount of $Al(OH)_3$, katoite, portlandite and $CaCO_3$ were quantified based on the measured weight loss between 200–300, 300–350, 350–450 and 600–900, respectively using the tangential method and the theoretical weight loss of solids [39].

PANalycatical X'Pert Pro MDF diffractometer equipped with an X'Celerator detector was used to record the X-ray powder diffraction patterns. Diffraction patterns were collected in increments of 5° from 70° 2θ at a conventional step size of 0.017° 2θ and a step measurement time of 460 s. The presence of different phases were determined with X'Pert HighScore Plus. The quantification of the amounts of the phases was carried out with calcium fluoride as external standard.

The solid phase composition in C—S—H was calculated by mass balance taking into account the initial quantities, the amount of Al, Ca, Si and Na in secondary phases if present and the fraction of Al, Ca, Si and Na in solution; the measurements and quantifications are also detailed in the appendix D.

The zeta potential was measured with an acoustophoresis electroacoustic method using a Zeta Probe from Colloid dynamics which is based on the frequency-dependent electroacoustic effect. The zeta potential is calculated from the frequency-dependent mobility using the O'Brien Equation. The calibration was made with potassium tungstosilicates, KSiW. To have the C—S—H particles in a homogeneous suspension, magnetic stirrer was used at 450 rpm during 10 min. A first measurement of zeta potential was made on unfiltered C—A—S—H samples. Then, a second measurement was carried out on the filtrated solutions to determine any interferences due to ions present in the solution which are considered as background and thus deducted from the initial measurement. The zeta potential is measured close to the interface between the stern layer and the diffusive layer giving the effective charge of the particle in suspension.

2.3. Thermodynamic modeling

Thermodynamic modelling was carried out using the Gibbs free energy minimization program *GEM*-Selektor [35,36]. The PSI-Nagra thermodynamic database [40] was used for thermodynamic data for aqueous species and portlandite and amorphous SiO_2. The solubility of microcrystalline $Al(OH)_3$, strätlingite, C—S—H and katoite was taken from the Cemdata18′. The concentrations in the C—S—H system were modelled using the CSHQ thermodynamic solid solution model [36].

The activity coefficients of the aqueous species γ_i were computed with the built-in extended Debye-Hückel equation with common ion-size parameter a_i = 3.31 Å for NaOH solutions and common third parameter b_y according to

$$\log \gamma_i = \frac{-A_y z_i^2 \sqrt{I}}{1 + B_y a_i \sqrt{I}} + b_y I$$

where z_i denotes the charge of species i, I the effective molal ionic strength, b_y is a semi-empirical parameter (~0.098 for NaOH electrolyte at 25 °C), and A_y and B_y are P,T-dependent coefficients. This activity correction is applicable up to ~1 M ionic strength [41].

The measured elemental concentrations of Al, Ca, Si and Na were used to calculate the saturation index (SI) of different solids according to SI = log IAP/K_{so}. The ion activity product (IAP) is calculated based on the measured concentrations in solution and K_{so} represents the theoretical solubility product of the solid. A saturation index above zero indicates that the solution is oversaturated with respect to this solid phase and that this phase could possibly precipitate. A negative value indicates undersaturation. The SI calculation was used to verify the solid phase composition found experimentally.

3. Results and discussion

3.1. The effect of pH on the Al uptake in C—S—H

Fig. 1 compares the measured aluminum in solution with the molar Al/Si in C—S—H obtained from mass balance calculations. Fig. 1 shows that the aluminum uptake in C—S—H increases with the dissolved aluminum concentrations at a Ca/Si ratio of a) 0.6, b) 0.8, c) 1.0, d) 1.2 and e) 1.4. A similar relation between aluminum uptake in C—S—H and dissolved aluminum in the solution has also been reported by [34] albeit at much higher aluminum concentrations (0.5 mmol/L to 3.5 mmol/L for Ca/Si = 0.95) and
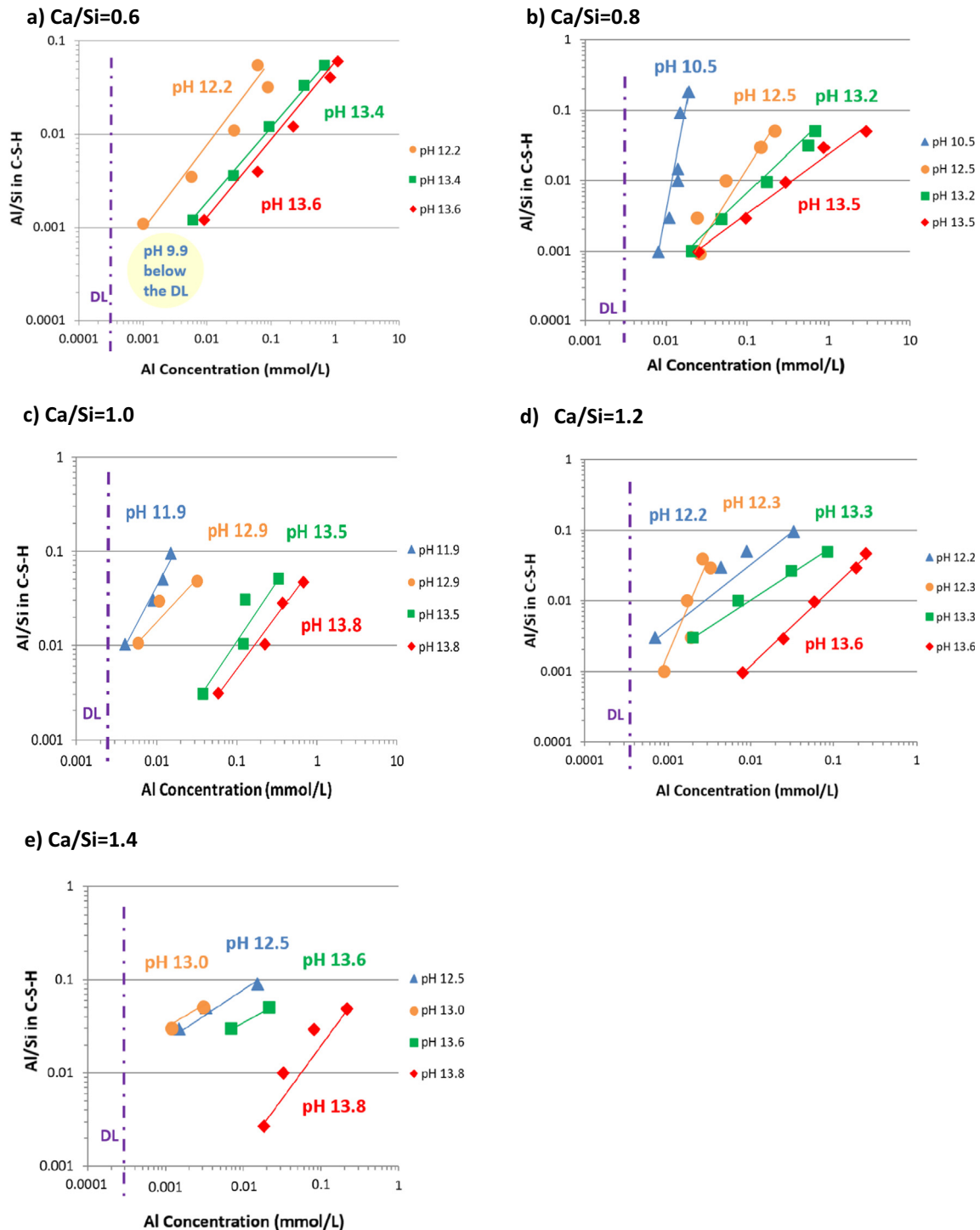
Fig. 1. The effect of the pH values on Al uptake in C—S—H after 3 months equilibration for Ca/Si ratios of a) 0.6; b) 0.8; c) 1.0; d) 1.2 and e) 1.4 in the absence of NaOH and in the presence of 0.1, 0.5 and 1 M NaOH.

by [32] at similar concentrations (0.021 mmol/L to 0.37 mmol/L for Ca/Si = 1.0). This clear relation between aluminum concentrations and Al/Si ratio in C—S—H indicates either a surface sorption of aluminum on the C—S—H [20] or the uptake in the C—S—H structure, which might be described by a solid solution model [42,43]. More information about the initial bulk position of each point can be found in appendix A.

The presence of alkali hydroxide increases the pH value, which is a key parameter in the system. The pH increases from 10.5 to 12.0 for the alkali free C—S—H up to 13.6 in the systems containing sodium hydroxide. Increasing the pH values lead to higher dissolved Al concentrations avoiding the precipitation of secondary phases such as aluminum hydroxide. Fig. 2 illustrates the strong dependence of dissolved aluminum concentrations in equilibrium with solid Al(OH)₃. 100 times higher dissolved Al concentrations can be reached at pH 13.5 than at pH 11.5 before aluminum hydroxide precipitation occurs.

The sorption isotherms in Fig. 1 show that in fact the presence of alkali hydroxide leads to much higher dissolved Al concentrations as the addition of NaOH increases the pH values and destabilizes
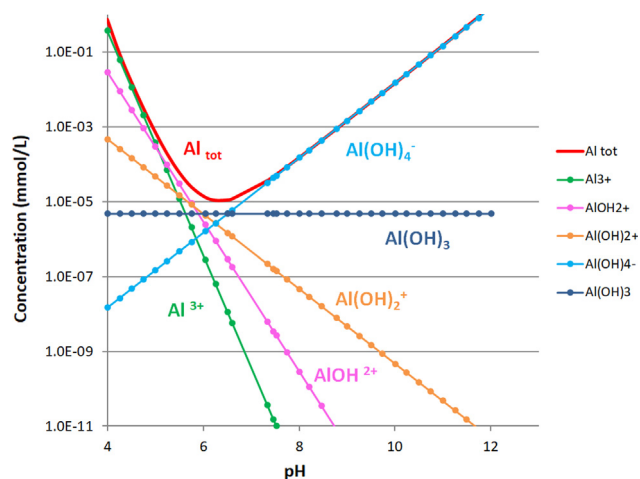
Fig. 2. The effect of pH on the calculated Al speciation in equilibrium with microcrystalline Al(OH)₃.

strätlingite and aluminum hydroxide. At all Ca/Si ratios investigated (0.6, 0.8, 1.0, 1.2 and 1.4, see Fig. 1) this effect of the pH value on the dissolved Al concentration is clearly visible. The presence of NaOH leads to a decrease in the amount of secondary phases such as Al(OH)₃ and katoite as discussed in section 3.4.

However, at the same aluminum concentrations, less aluminum uptake in C—S—H is observed in the presence of alkali hydroxide. This suppression of aluminum uptake is stronger at higher pH values. This could be related to i) the increase of the fraction of the thermodynamically stable aqueous aluminum hydroxide complex $(Al(OH)_{4 (aq)}^-)$ in solution and/or ii) the increase of the negative surface charge of C—S—H due to the pH increase, i.e. the interaction of the negatively charged complex $(Al(OH)_{4 (aq)}^-)$ in solution with the negatively charged surface will lower the tendency for aluminum incorporation. The speciation of aqueous aluminum depends on the pH values as shown in Fig. 2; negatively charged $[Al(OH)_4^-]$ dominates the speciation at pH > 7 [44]. The fraction of the Al $(OH)_4^-$ species increases with the pH values, which lowers the tendency of Al to be sorbed by C—S—H. Lower aluminum uptake in C—S—H at high NaOH concentrations could also be related to the decrease of the occurrence of filled bridging position with increasing pH. Si Nuclear magnetic resonance (NMR) measurements have shown shorter silica chain length at high pH values [17].

Zeta potential measurements are shown in Fig. 3. The zeta potential measures the charge of a particle not directly at the surface but in some distance; such that ions near the surface and even some in the diffuse layer, contribute to the measured charge [44,45]. The zeta potential measurements of C—S—H show a negative charge for low Ca/Si C—S—H and thus at low calcium concentrations. At higher calcium concentrations, the measured zeta potential increases from negative values to positive values, as the calcium accumulates near the surface of C—S—H as discussed in detail in [20]. As the increase of calcium concentrations at higher Ca/Si in the C—S—H is also accompanied by an increase of pH value, this charge reversal can also be observed as a function of pH as shown by the circles in Fig. 3, which represents measured zeta potentials on C—S—H with Ca/Si = 0.66 to 1.51, in the absence of any alkali hydroxide [20].

However, an increase of the pH value at constant Ca/Si has the opposite effect. It lowers the measured zeta potential to more negative values as illustrated by the squares in Fig. 3, where the measured zeta potential decreases from −0.5 for Ca/Si = 1.0 and no alkali to −18.4 in the presence of 0.15 M KOH as reported by [32]. This effect is also visible in the difference between the zeta potential values measured in the absence of alkali (blue circles) and those in the presence of 0.1 M NaOH (red triangles); for Ca/Si 1.0, the measured zeta potential decreases from 1 in the absence of NaOH to −14 mV. This is related to an increased deprotonation of the silanol sites at higher pH values, in agreement with the trends predicted by molecular modelling [46].

Measurements of the zeta potential in 0.1 M NaOH of C—S—H with Ca/Si ratio from 0.6 to 1.6 (red triangles) confirmed the effect of pH values on the measured zeta potential, all data were significantly lower than in the absence of NaOH indicating a more negative C—S—H surface at higher pH values. Even at higher pH values an increase of the Ca/Si ratio of C—S—H increased the zeta potential from −27 to −3 mV (from full triangles to empty ones) as the calcium concentrations increase with the Ca/Si in the C—S—H, as discussed in the next section. Thus, also in the presence of 0.1 M NaOH increasing the Ca/Si ratio decreases the negative charge near the C—S—H particles which leads to an increase in measured zeta potentials. The measured zeta potential is in addition influenced by the concentration of Na⁺ cations, which can also be present near the surface of C—S—H. As Ca²⁺ and Na⁺ cations compete to compensate the negative charge [13], at high NaOH concentration Na⁺ can replace some of the Ca²⁺ near the C—S—H surface thus lowering the measured zeta potential. At higher alkali hydroxide concentrations
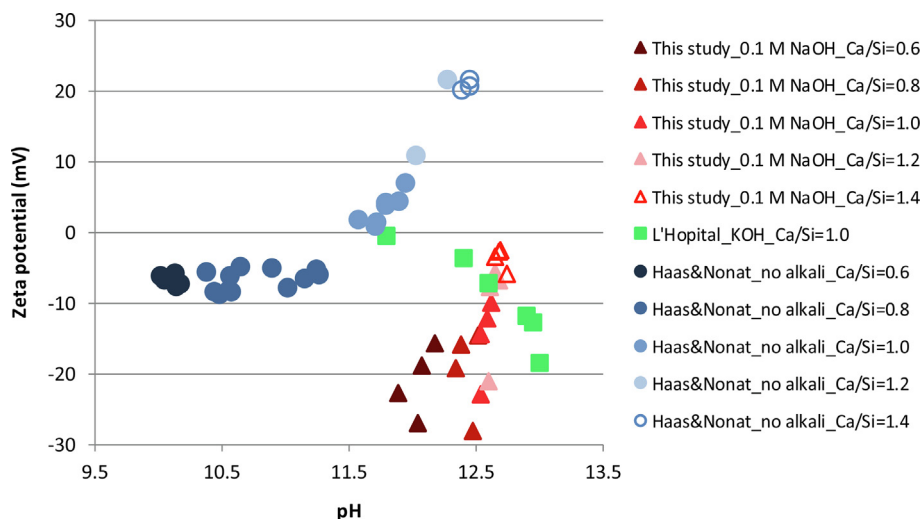

Fig. 3. Zeta potential measurements for C—S—H samples in the absence of alkali hydroxide (circles; [20]), the effect of 0 to 0.15 M KOH (squares; [32]), and in the presence of 0.1 M NaOH (triangles; this study).

(0.5 and 1 M NaOH), however, the zeta potential measurements are strongly affected by the increase in ionic strength which moves the distance where the zeta potential is measured, such that the experimental values show a very high scatter and a reliable measurement is not possible (data not shown). The different shading of the triangles and circles correspond to the different Ca/Si ratios; for each Ca/Si at 0.1 M NaOH several measurements were available corresponding to the different Al/Si ratios from 0 to 0.2. The different experiments are also the reason for the slight difference in the pH values for Ca/Si = 0.6 from 11.9 to 12.2.

The zeta potential measurements illustrate that higher pH values at constant Ca/Si result in a more negatively charged C—S—H surface due to the deprotonation of the silanol sites. Together, the more negative surface charge and the increasing predominance of aqueous $Al(OH)_4^-$ complexes suppresses Al uptake by C—S—H at high pH values as discussed above and as visible in the data shown in Fig. 1.

3.2. The effect of pH on the aqueous phase composition

Fig. 4 shows the effect of sodium hydroxide on the aqueous phase composition at 5 different Ca/Si ratios of a) 0.6, b) 0.8, c) 1.0, d) 1.2 and e) 1.4. In a first approximation, the measured dissolved Ca and Si concentrations in Fig. 4 are compared to thermodynamic predictions using the CSHQ solid solution model for C—S—H [36,47]. The CSHQ model was used as it is able to model the entire Ca/Si range investigated instead of the CNASH model developed by [42,43] as the CNASH model concentrates on low Ca/Si.

The alkali free C—S—H are the data points at pH 10, 10.5, 11.9, 12 and 12.2 for Ca/Si ratio of 0.6, 0.8, 1.0, 1.2 and 1.4, respectively. A comparison of the alkali free C—S—H in Fig. 4a-e illustrates that the Ca concentrations increase with increasing Ca/Si and the Si concentrations decrease; both these trends as well as the measured concentrations agree well with other solubility measurements of C—S—H published in literature as summarized in [13,48].

As it is shown in Fig. 4, higher pH values increase the concentrations of silica and aluminum in solution, while the calcium concentration decreases. The same trends have been observed for C—S—H and C—A—S—H systems in the presence of different quantities of sodium and potassium hydroxide [17,32,49,50].

Increasing the pH values leads to a decrease in Ca concentrations in the solution; this decreasing trend in calcium concentrations agrees well with the modeling predictions although the model overestimates somewhat the measured Ca concentrations at low Ca/Si ratios and underestimates them at Ca/Si = 1.2. At Ca/Si = 1.4, the calcium concentrations above pH of 12.5 are determined by the solubility of portlandite as shown in Fig. 4e.

In contrast to the calcium, the silica concentration increase with the pH values (Fig. 4). At low Ca/Si ratios this behavior is dominated by the increase of the amorphous silica solubility with pH. At intermediate Ca/Si ratios, the increase of dissolved Si is related to the decrease of the dissolved Ca concentration and the common ion effect with respect to C—S—H.

The measured Al concentrations increase with the amount of Al present in the system as visible in Fig. 4a-e, where the different symbols represent samples with different Al/Si ratios from 0.001 to 0.05. The formation of $SiO(OH)_3^-$, $SiO_2(OH)_2^{2-}$ and $AlOH_4^-$ complexes at higher pH values increases the silicon and aluminum concentrations as illustrated for aluminum in Fig. 2. This simultaneous increase of Si, Al and hydroxide concentrations with pH lowers the calcium concentrations due to the common ion effect with C—S—H, katoite and/or portlandite. Increasing the pH values increased the Al concentrations in the aqueous solution at all Ca/Si ratios similarly to the Si concentrations, which could indicate a comparable uptake mechanism for Si and Al in C—S—H both at high and low

Ca/Si. In fact, an uptake of Al^{IV} in the silica chain as observed at low Ca/Si, can be expected to result in similar trends of Si and Al concentrations upon variation of pH values and Ca/Si ratios. These results tentatively indicate that also six-fold coordinated Al^{VI}, the dominant Al species at high Ca/Si, could be associated with the silica chain [13,26,31], in agreement with recent findings from molecular modeling and with the observed increase of the silica chain length in the presence of Al [17].

3.3. The effect of Ca/Si ratio on the Al uptake in C—S—H

The Ca/Si ratio in C—S—H affects not only the aluminum concentrations but also the amount of Al taken up in C—S—H. Fig. 5 shows the effect of Ca/Si ratios on Al uptake in C—S—H for different systems; a) in the absence of sodium hydroxide, b) in the presence of 0.1 M NaOH and c) in the presence of 1 M NaOH. Fig. 5a shows that in the absence of any alkali hydroxide, the maximum aluminum concentrations in solution are < 0.03 mmol/L, limited by the precipitation of $Al(OH)_3$ and katoite, which restrains the maximum molar Al/Si to ≈ 0.1. Fig. 5a also indicates that at higher Ca/Si ratios more Al is taken up in C—S—H for the samples without alkali hydroxide, in particular at very low aluminum concentrations. For a given Al concentration, the Al uptake in C—S—H is increasing when we move from Ca/Si = 0.8 to Ca/Si = 1.4. In contrast, the uptake is similar at Al concentrations above 0.01 mM. In addition, a different uptake regime is observed at high and at low Ca/Si ratios. The slope of the line between dissolved Al and Al in C—S—H is much steeper for samples at Ca/Si ratio of 0.8 compared to those at Ca/Si of 1.0 and above. A comparable difference between the Al uptake by low Ca/Si and high Ca/Si C—S—H is also observed in 0.1 M NaOH (Fig. 5b). At low aluminum concentrations (< 0.01 mM) increasing Ca/Si ratio leads to an increase of the Al uptake in C—S—H. This might be related to the presence of different Al environments at low Ca/Si ratios and high Ca/Si ratios. ^{27}Al MAS (NMR) have indicated that four-fold coordinated Al^{IV} is the dominant environment in low Ca/Si C—S—H, while at higher Ca/Si ratios six-fold coordinated Al^{VI} is dominant [13,17,26,27,30,31]. The position of six-fold coordinated Al^{VI}, which is also known as TAH (third aluminate hydrate), is discussed controversially in literature; it has been suggested to be present either on the surface or in the bridging site [25]. However, how these different Al environments in C—S—H affect the Al uptake is presently not well investigated. Possibly the presence of more calcium in the interlayer at higher Ca/Si ratios and the resulting apparent positive charge on the C—S—H surface could ease the uptake of $Al(OH)_4^-$. Such a stabilizing effect of Ca on Al uptake would be consistent with a recent X-ray adsorption near edge structure (XANES) study, where an ordering of the Ca in the interlayer was observed in the presence of Al [23]. However, in addition also kinetic restraints could be important, and the equilibration time could be different at low Ca/Si and high Ca/Si.

Fig. 5c shows the effect of the Ca/Si ratio on Al uptake in C—S—H for samples with 1 M NaOH. Increasing the Ca/Si ratios leads to a decrease in Al concentration in solution and an increase in Al uptake in C—S—H as also observed for the samples without NaOH. At an Al concentration of 0.01 mmol/L, an Al/Si of 0.003 is observed for low Ca/Si C—S—H, which increases to Al/Si = 0.05 at Ca/Si = 1.2. However, little difference is observed between the Ca/Si ratio of 0.6 and 0.8 and between Ca/Si ratios of 1.2 and 1.4 for samples with 1 M NaOH. Moreover, the uptake of Al in the samples at Ca/Si ratio of 0.6 (for 0.1 M and 1 M NaOH) do not show the same trend compared to the case of Ca/Si ratio of 0.8. The reason for this behavior cannot be explained. Both at 0.5 M NaOH (data not shown) and at 1 M NaOH the slope has a comparable steepness independent of the Ca/Si ratio in contrast to the observation at lower pH values. The reasons for this different behavior are presently unknown but points towards different binding sites for Al in C—S—H. Further
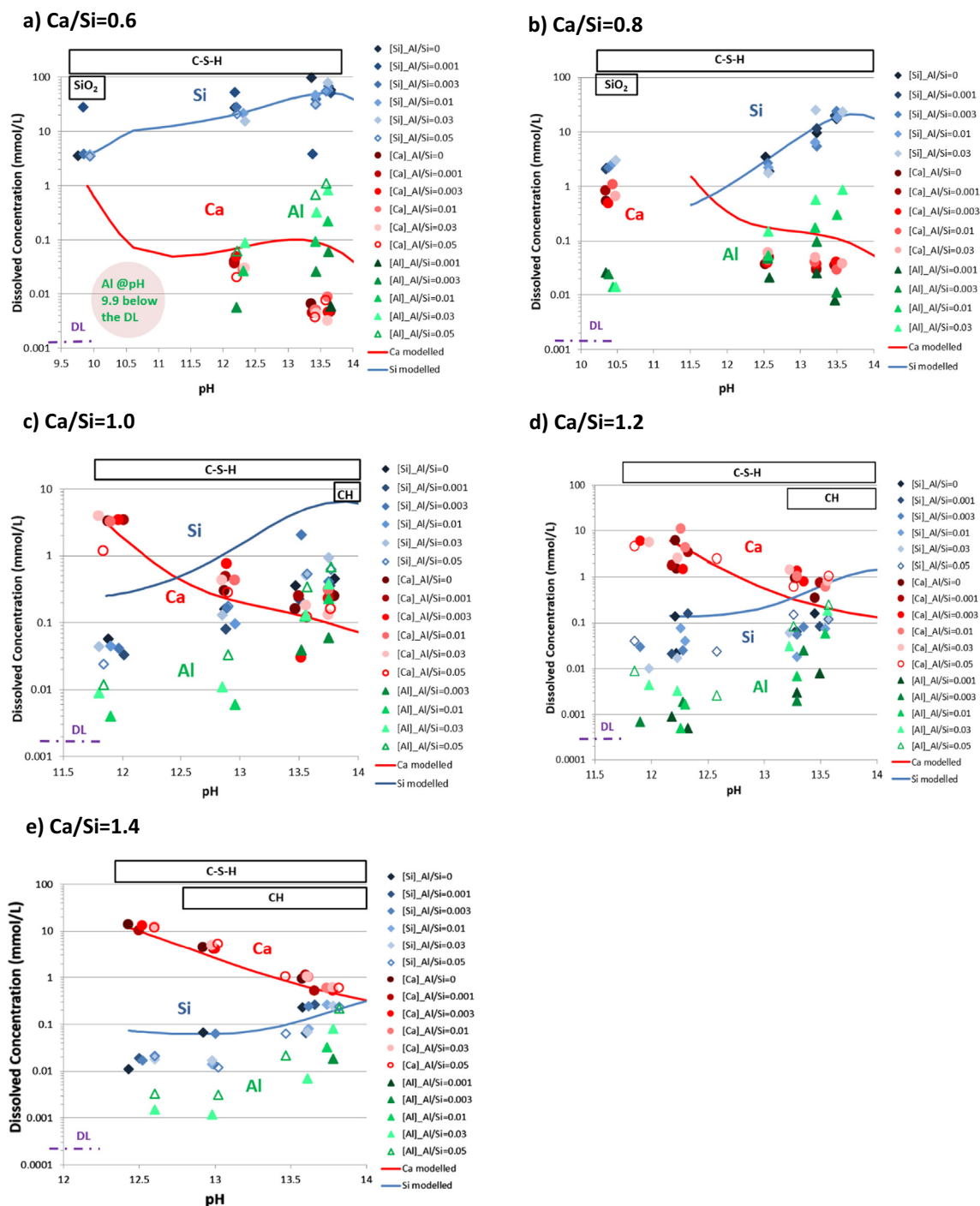
Fig. 4. The effect of pH on aqueous phase composition at Ca/Si ratio of a) 0.6; b) 0.8; c) 1.0; d) 1.2 and e) 1.4. (Points represent experimental data and lines are the calculated values using the CSHQ model [36]).

detailed studies of Al-binding in C—S—H by spectroscopic methods at different Al concentrations and pH values are needed, which is presently carried out in parallel projects [23].

3.4. Solid phase analysis

Thermogravimetric analysis was used to investigate whether the secondary phases are formed in the presence of additional aluminum. Fig. 6 shows the TGA results for samples at Ca/Si ratio of 1.4 with no alkali at different Al/Si ratios. At the highest Al/Si ratio

(Al/Si = 0.1), the presence of a low amount of aluminum hydroxide (Al(OH)$_3$) is observed. It is also obvious from Fig. 6 that an increase in the initial Al/Si ratios increases the quantities of secondary phases such as aluminum hydroxide (from 0% Al(OH)$_3$ at Al/Si = 0.03 and 0.05 to 0.58% Al(OH)$_3$ at Al/Si = 0.1). The amount of secondary phases quantified by TGA was used to assess the amount of Ca, Si and Al in C—S—H using mass balance calculations. In many cases at higher Al/Si ratios, the Al/Si ratios in C—S—H are smaller than the total Al/Si ratios in solid due to the presence of katoite and aluminum hydroxide. However, at lower Al/Si ratios,
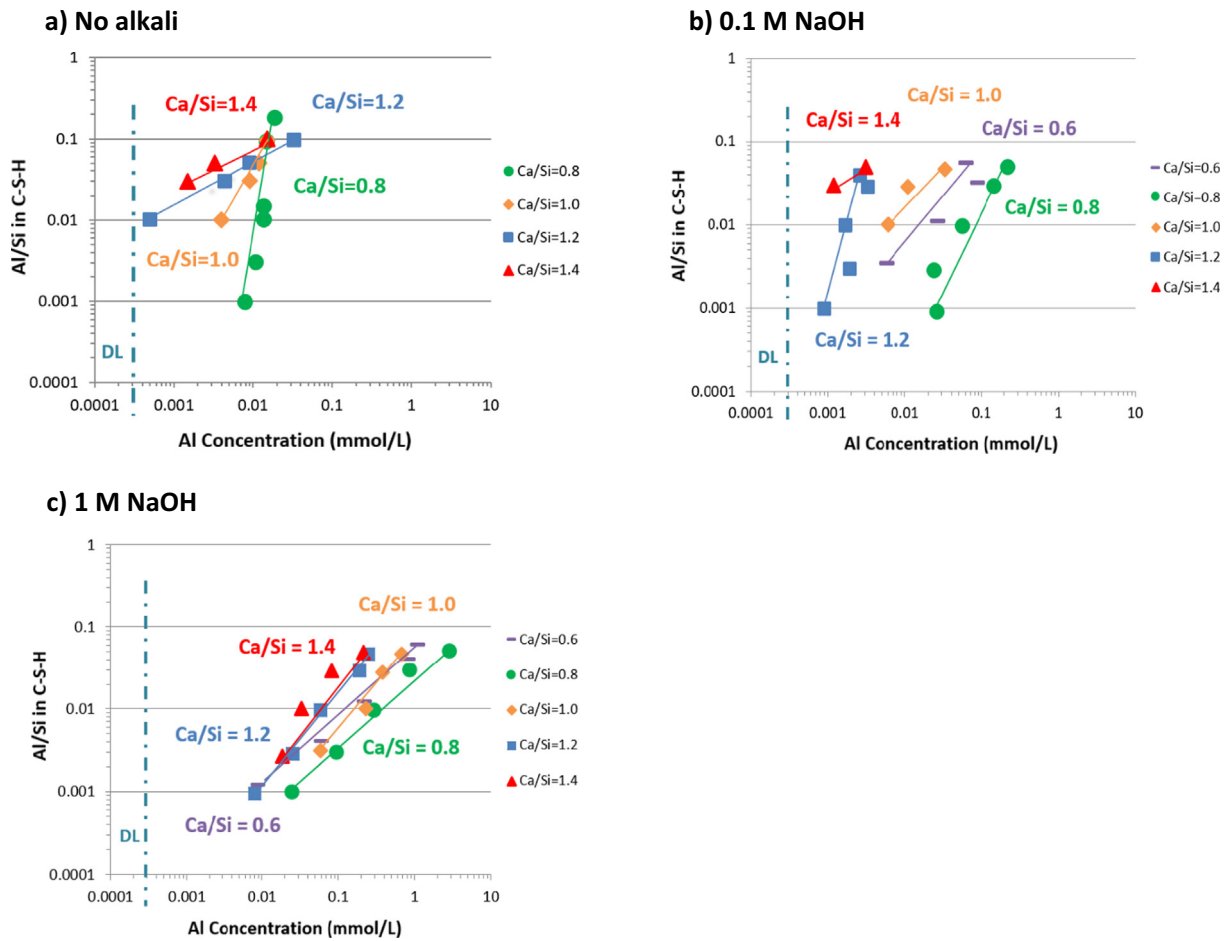
Fig. 5. The effect of Ca/Si ratio on the Al uptake in C—S—H for samples a) without alkali hydroxide (The data at Ca/Si = 0.6 were below the detection limit); b) 0.1 M NaOH and c) 1 M NaOH. (The lines are added as eye guide only).
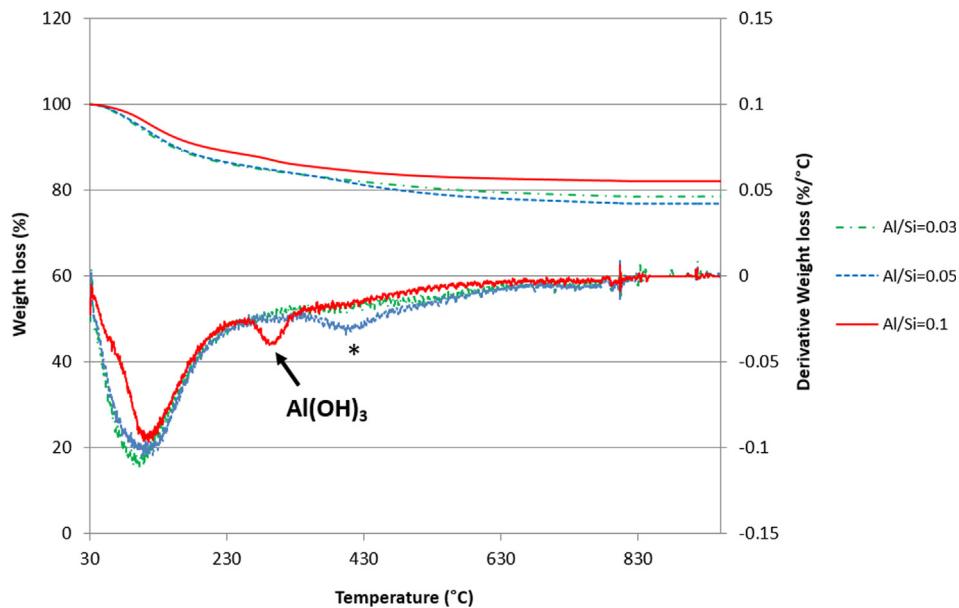

Fig. 6. The TGA results for samples at Ca/Si ratio of 1.4 with no alkali at different Al/Si ratios (*: The hump around 430 °C could not be assigned to a solid and was thus tentatively assigned to thermal decomposition of C—N—A—S—H [51]).

no other phases are observed, such that the Al/Si ratio in C—S—H is the same as the total ratio in solid. More details regarding the values of secondary phases in solid as well as the Al/Si ratios in C—S—H can be found in Appendix A. The hump around 430 °C could not be assigned to a solid and was thus tentatively assigned to thermal decomposition of C—N—A—S—H [51].
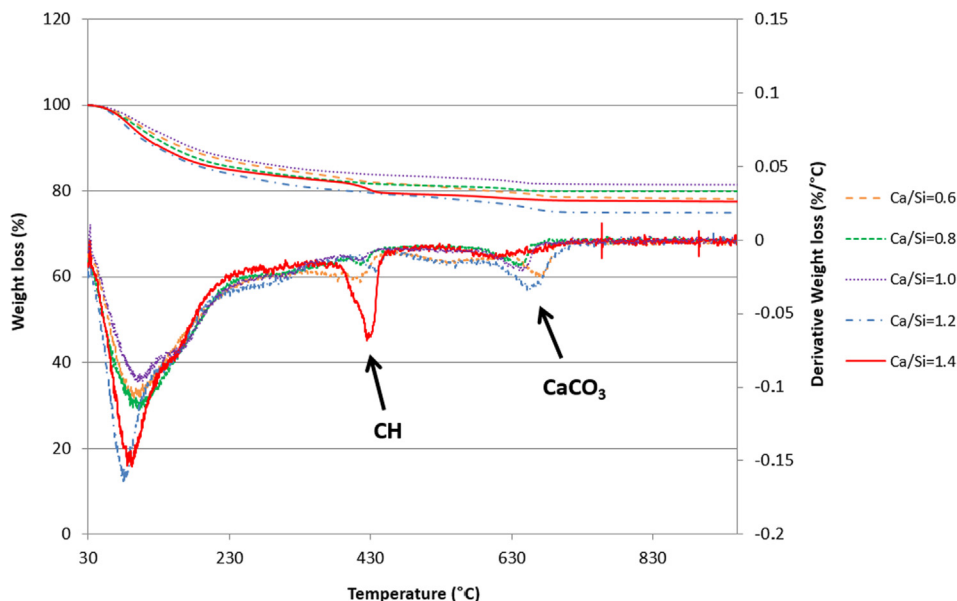
Fig. 7. The TGA results for samples at Al/Si ratio of 0.03 with 1 M NaOH and different Ca/Si ratios.

Fig. 7 illustrates the effect of Ca/Si on the phases present for samples with Al/Si ratio = 0.03 and 1 M NaOH. At higher Ca/Si ratios the presence of high amount of portlandite is observed (note that amorphous silica, which might be present at low Ca/Si and the absence of NaOH, cannot be detected by TGA [33]). Due to the high pH in 1 M NaOH solutions, portlandite is observed at Ca/Si = 1.2 (0.22 wt% portlandite) and at Ca/Si = 1.4 (1.85 wt%). In the absence of NaOH, no portlandite is observed at Ca/Si = 1.2 and 1.4 in agreement with earlier observations [17,48]. The formation of portlandite at high NaOH concentrations and at higher Ca/Si also explains the decrease in the dissolved calcium concentrations at increasing pH values shown in Fig. 4.

From the measured aqueous concentrations, saturation indexes (SI) were calculated as an independent method to verify the presence of secondary phases in the solid samples. The SI values for different secondary phases such as portlandite, amorphous silica, microcrystalline aluminum hydroxide, strätlingite and katoite are compiled in appendix D. All the solutions were near saturation with respect to C—S—H (the calculated SI values were generally in the range of ± 0.5). In the absence of NaOH the solution were also saturated with respect to amorphous SiO_2 at low Ca/Si (Ca/Si = 0.6) but in all cases significantly undersaturated with respect to portlandite, in agreement with the TGA data. The presence of NaOH led to undersaturation with respect to amorphous SiO_2 (even at Ca/Si = 0.6) and stabilized portlandite at Ca/Si = 1.2 and 1.4, again in agreements with the TGA data. At higher Ca/Si ratios the presence of portlandite is observed. At Ca/Si ratios of 0.6 and 0.8, , the presence of additional very broad TGA signals in the range of 250 to 450 °C are observed, which was tentatively assigned to thermal decomposition of C—N—A—S—H [51] and the presence of a minor amount of portlandite. The addition of aluminum, led in the absence of NaOH near to saturation with respect to microcrystalline $Al(OH)_3$ at higher Al concentration at Ca/Si = 0.8 in agreement with the TGA data, but the solution remained undersaturated at Ca/Si = 1.4, although TGA indicated the presence of a minor amount of $Al(OH)_3$. All solutions were undersatured with respect to katoite and strätlingite, although katoite has been observed in some of the samples. A similar observation (presence of katoite although the solutions were clearly understaturated) has been made by [32] and has been related to a kinetically very

slow dissolution of katoite which has formed early in the experiments.

Fig. 8 shows the XRD pattern for samples at Al/Si ratio of 0.03 with 1 M NaOH at different Ca/Si ratios. At higher Ca/Si ratios, the presence of significant amount of portlandite is observed; in agreement with our observation in Fig. 7. However, at low Ca/Si ratios a small amount of portlandite is also visible. Also, TGA results in Fig. 7 indicate the presence of very low amount of portlandite at Ca/Si ratio of 0.6. As it is mentioned before, this can be due to non-equilibrium condition of system.

Fig. 9 shows the TGA results for samples at Ca/Si ratio of 0.8 and Al/Si ratio of 0.03 with different NaOH concentrations. For the sample without NaOH, the presence of a low amount of $Al(OH)_3$ and katoite was observed. However, at higher NaOH concentrations (0.1, 0.5 and 1 M) no secondary phases were present, in agreement with Fig. 1 which illustrates that the presence of NaOH increases the pH values and destabilizes aluminum hydroxide. At higher alkali hydroxide concentrations, more Al is present in solution due to the preferred formation of $Al(OH)_4^-$ complex which leads to the less secondary phases and less Al in C—S—H.
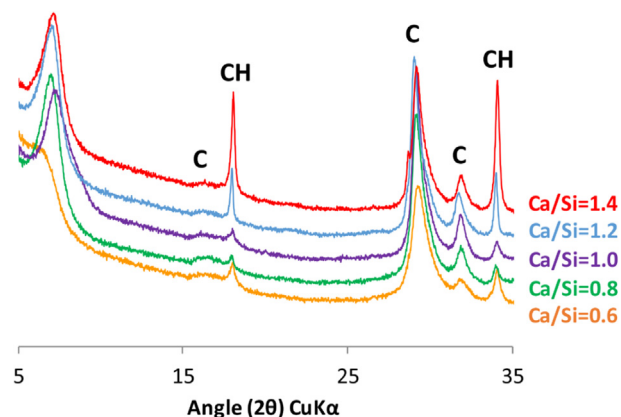

Fig. 8. The XRD patterns for samples at Al/Si ratio of 0.03 with 1 M NaOH and different Ca/Si ratios.
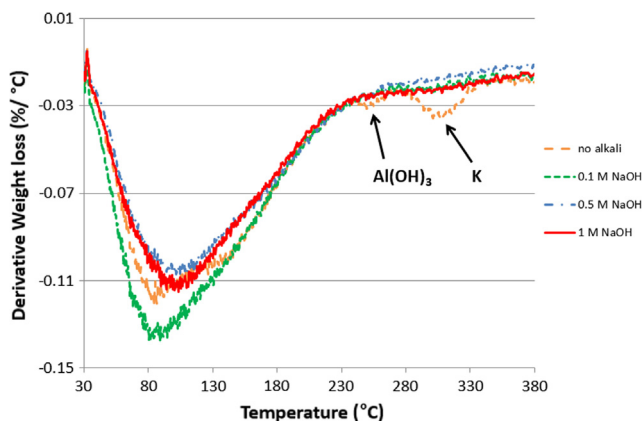
Fig. 9. The TGA results for samples at Al/Si ratio of 0.03 and Ca/Si ratio of 0.8 with different NaOH concentrations.

4. Conclusion

The effect of pH, Ca/Si ratio and aluminum concentration on the aluminum uptake by C—S—H was investigated experimentally. The aluminum uptake in C—S—H increases with the aluminum concentrations in solution. In the absence of alkali hydroxide, however, the maximum aluminum concentrations in solution are limited to approximately < 0.03 mmol/L by the precipitation of $Al(OH)_3$ and katoite, which limits the maximum molar Al/Si to ≈ 0.1. The use of ICP-OES and ICP-MS measurements in this paper enables us to record the Al uptake in C—S—H systems at very low Al concentrations, which allowed for the first time to assess the effect of pH and Ca/Si. The results of previous studies were limited by the small experimental range between the detection limit in the range of 0.004 mmol/L and the precipitation of secondary phases at Al concentrations of 0.03 mmol/L and above [17,23,32-34,51].

The presence of sodium hydroxide increases the pH values, which prevents aluminum hydroxide formation, and thus leads to much higher dissolved Al concentration of up to 2 mmol/L. The increase of the Al uptake in C—S—H, however, is limited as high pH values suppress Al uptake in C—S—H. Zeta potential measurements (Fig. 3) and molecular modelling [46] indicate that at higher pH values the C—S—H surface is more negatively charged due to increased deprotonation of the silanol sites, which suppresses Al uptake, as the main hydroxide complex of aluminum above pH of 7, $Al(OH)_4^-$, is also negatively charged. In addition, the fraction of the $Al(OH)_4^-$ aqueous complex increases also with the pH values (Fig. 2), which further lowers the tendency of Al to be sorbed by C—S—H.

The aluminum uptake in C—S—H is also influenced by the Ca/Si ratios. Increasing the Ca/Si ratios increase the Al uptake in C—S—H, while the dissolved Al concentrations decrease such that at constant Al concentration in the solution more Al is taken up in C—S—H at higher Ca/Si ratios. This could be related to a stabilization of aluminum in the C—S—H interlayer in the presence of calcium in agreement with a recent XANES study, where the presence of Al had an ordering effect on Ca in the interlayer [23].

Increasing the pH values and/or decreasing the Ca/Si in C—S—H increased not only the Al concentrations but in parallel also the Si concentrations in solution. This similar behavior of Al and Si towards changes in pH points toward the uptake of aluminum within the silica chain both at high and low Ca/Si. This agrees well with solid state Si NMR results which indicate that at low Ca/Si C—S—H Al^{IV} is present in the bridging sites of the silica chain. The results tentatively indicate that also six-fold coordinated Al^{VI}, the dominant Al species at high Ca/Si, could be present within the silica chain.

For the further development of thermodynamic models for C—S—H containing Al, a comprehensive knowledge about the sorption at varying Al concentrations is needed. The gained fundamental knowledge on the effect of pH and Ca/Si on Al uptake in C—S—H phases and on Al substitution mechanisms can be transferred to calcium silicate hydrates beyond the field of cement chemistry. The consideration of Al-substituted C—S—H phases in thermodynamic modelling will have a significant impact on the reliability of calculating the composition and phase assemblages of Portland cements blended with supplementary cementitious materials and in understanding the different factors affecting their durability.

Declaration of Competing Interest

The authors declare that they have no known competing financial interests or personal relationships that could have appeared to influence the work reported in this paper.

Acknowledgements

Appendix A. Supplementary data

Supplementary data to this article can be found online at https://doi.org/10.1016/j.jcis.2020.03.057.

References

[1] S.A. Miller, R.J. Myers, Environmental Impacts of Alternative Cement Binders, Environ. Sci. Technol. 54 (2020) 677–686.
[2] E. Gartner, I. Maruyama, J. Chen, A new model for the C-S-H phase formed during the hydration of Portland cements, Cem. Concr. Res. 97 (2017) 95–106.
[3] L.D. Ellis, A.F. Badel, M.L. Chiang, R.J.-Y. Park, Y.-M. Chiang, Toward electrochemical synthesis of cement—An electrolyzer-based process for decarbonating CaCO 3 while producing useful gas streams, Proc. Natl. Acad. Sci. 201821673 (2019).
[4] J. Li, G. Geng, W. Zhang, Y.S. Yu, D.A. Shapiro, P.J.M. Monteiro, The Hydration of β- And α′ H -Dicalcium Silicates: An X-ray Spectromicroscopic Study, ACS Sustain. Chem. Eng. 7 (2019) 2316–2326.
[5] E. Gartner, Industrially interesting approaches to "low-CO2" cements, Cem. Concr. Res. 34 (2004) 1489–1498.
[6] M. Thomas, L. Barcelo, B. Blair, K. Cail, A. Delagrave, K. Kazanis, Lowering the carbon footprint of concrete by reducing clinker content of cement, Transp. Res. Rec. 99–104 (2012).
[7] P.J.M. Monteiro, S.A. Miller, A. Horvath, Towards sustainable concrete, Nat. Mater. 16 (2017) 698–699.
[8] B. Lothenbach, K. Scrivener, R.D. Hooton, Supplementary cementitious materials, Cem. Concr. Res. 41 (2011) 1244–1256.
[9] J. Li, W. Zhang, C. Li, P.J.M. Monteiro, Green concrete containing diatomaceous earth and limestone: Workability, mechanical properties, and life-cycle assessment, J. Clean. Prod. 223 (2019) 662–679.
[10] I. Baur, C. Ludwig, C. Annette Johnson, The leaching behavior of cement stabilized air pollution control residues: A comparison of field and laboratory investigations, Environ. Sci. Technol. 35 (2001) 2817–2822.
[11] C. Ludwig, C.A. Johnson, M. Käppeli, A. Ulrich, S. Riediker, Hydrological and geochemical factors controlling the leaching of cemented MSWI air pollution control residues: A lysimeter field study, J. Contam. Hydrol. 42 (2000) 253–272.
[12] I.G. Richardson, The nature of C-S-H in hardened cements, Cem. Concr. Res. 29 (1999) 1131–1147.
[13] B. Lothenbach, A. Nonat, Calcium silicate hydrates : Solid and liquid phase composition, Cem. Concr. Res. 78 (2015) 57–70.
[14] M. Antoni, J. Rossen, F. Martirena, K. Scrivener, Cement substitution by a combination of metakaolin and limestone, Cem. Concr. Res. 42 (2012) 1579–1589.
[15] C. Li, H. Zhu, M. Wu, K. Wu, Z. Jiang, Pozzolanic reaction of fly ash modified by fluidized bed reactor-vapor deposition, Cem. Concr. Res. 92 (2017) 98–109.
[16] C. Li, M. Wu, Q. Chen, Z. Jiang, Chemical and mineralogical alterations of concrete subjected to chemical attacks in complex underground tunnel environments during 20–36 years, Cem. Concr. Compos. 86 (2018) 139–159.

[17] E. L'Hôpital, B. Lothenbach, D.A. Kulik, K. Scrivener, Influence of calcium to silica ratio on aluminium uptake in calcium silicate hydrate, Cem. Concr. Res. 85 (2016) 111–121.
[18] L. Irbe, R.E. Beddoe, D. Heinz, The role of aluminium in C-A-S-H during sulfate attack on concrete, Cem. Concr. Res. 116 (2019) 71–80.
[19] G.L. Kalousek, Crystal Chemistry of Hydrous Calcium Silicates, J. Am. Ceram. Soc. 40 (1956) 74–80.
[20] J. Haas, A. Nonat, From C-S-H to C-A-S-H: Experimental study and thermodynamic modelling, Cem. Concr. Res. 68 (2015) 124–138.
[21] E. Bonaccorsi, S. Merlino, A.R. Kampf, The crystal structure of tobermorite 14 Å (plombierite), a C-S-H phase, J. Am. Ceram. Soc. 88 (2005) 505–512.
[22] S. Merlino, E. Bonaccorsi, T. Armbruster, Tobermorites: Their real structure and order-disorder (OD) character, Am. Mineral. 84 (1999) 1613–1621.
[23] J. Li, G. Geng, R. Myers, Y.S. Yu, D. Shapiro, C. Carraro, R. Maboudian, P.J.M. Monteiro, The chemistry and structure of calcium (alumino) silicate hydrate: A study by XANES, ptychographic imaging, and wide- and small-angle scattering, Cem. Concr. Res. 115 (2019) 367–378.
[24] S. Ortaboy, J. Li, G. Geng, R.J. Myers, P.J.M. Monteiro, R. Maboudian, C. Carraro, Effects of CO2 and temperature on the structure and chemistry of C-(A-)S-H investigated by Raman spectroscopy, RSC Adv. 7 (2017) 48925–48933.
[25] I.G. Richardson, A.R. Brough, R. Brydson, G.W. Groves, C.M. Dobson, Location of aluminium in substituted calcium silicate hydrate (C-S-H) gels as determined by Si-29 and Al-27 NMR and EELS, J. Am. Ceram. Soc. 76 (1993) 2285–2288.
[26] G. Renaudin, C. Cau-dit-Coumes, J. Russias, F. Frizon, F. Leroux, Structural characterization of C-S-H and C-A-S-H samples—Part II: Local environment investigated by spectroscopic analyses, J. Solid State Chem. 182 (2009) 3320–3329.
[27] G.K. Sun, J.F. Young, R.J. Kirkpatrick, The role of Al in C-S-H: NMR, XRD, and compositional results for precipitated samples, Cem. Concr. Res. 36 (2006) 18–29.
[28] M. Daugaard Andersen, H.J. Jakobsen, Jø. Skibsted, Incorporation of aluminum in the calcium silicate hydrate (C-S-H) of hydrated Portland cements: A high-field 27Al and 29Si MAS NMR investigation, Inorg. Chem. 42 (2003) 2280–2287.
[29] M.D. Andersen, H.J. Jakobsen, J. Skibsted, A new aluminium-hydrate species in hydrated Portland cements characterized by 27Al and 29Si MAS NMR spectroscopy, Cem. Concr. Res. 36 (2006) 3–17.
[30] P. Faucon, A. Delagrave, C. Richet, H. Zanni, J.M. Marchand, Aluminum Incorporation in Calcium Silicate Hydrates (C–S–H) Depending on Their Ca/Si Ratio, J. Phys. Chem. B. 103 (2002) 7796–7802.
[31] X. Pardal, F. Brunet, T. Charpentier, I. Pochard, A. Nonat, 27Al and 29Si solid-state NMR characterization of calcium-aluminosilicate-hydrate, Inorg. Chem. 51 (2012) 1827–1836.
[32] E. L'Hôpital, B. Lothenbach, G. Le Saout, D. Kulik, K. Scrivener, Incorporation of aluminium in calcium-silicate-hydrates, Cem. Concr. Res. 75 (2015) 91–103.
[33] E.L. Hôpital, B. Lothenbach, K. Scrivener, D.A. Kulik, Alkali uptake in calcium alumina silicate hydrate (C-A-S-H), Cem. Concr. Res. 85 (2016) 122–136.
[34] X. Pardal, I. Pochard, A. Nonat, Experimental study of Si-Al substitution in calcium-silicate-hydrate (C-S-H) prepared under equilibrium conditions, Cem. Concr. Res. 39 (2009) 637–643.
[35] T. Wagner, D.A. Kulik, F.F. Hingerl, S.V. Dmytrievava, Gem-selektor geochemical modeling package: TSolMod library and data interface for multicomponent phase models, Can. Mineral. 50 (2012) 1173–1195.
[36] D.A. Kulik, Improving the structural consistency of C-S-H solid solution thermodynamic models, Cem. Concr. Res. 41 (2011) 477–495.
[37] A. Vollpracht, B. Lothenbach, R. Snellings, J. Haufe, The pore solution of blended cements: a review, Mater. Struct. Constr. 49 (2016) 3341–3367.
[38] B. Lothenbach, F. Winnefeld, Thermodynamic modelling of the hydration of Portland cement, Cem. Concr. Res. 36 (2006) 209–226.
[39] K. Scrivener, R. Snellings, B. Lothenbach, A Practical Guide to Microstructural Analysis of Cementitious, Materials, 2015.
[40] T. Thoenen, W. Hummel, U. Berner, E. Curti, The PSI/Nagra Chemical Thermodynamic Database 12/07 Nuclear Energy and Safety Research Department Laboratory for Waste Management (LES), (2014).
[41] B. Planer-friedrich, Nordstrom A Practical Guide to Modeling of Natural and Contaminated Aquatic Systems, 2008.
[42] R.J. Myers, S.A. Bernal, J.L. Provis, A thermodynamic model for C-(N-)A-S-H gel: CNASH-ss. Derivation and validation, Cem. Concr. Res. 66 (2014) 27–47.
[43] R.J. Myers, B. Lothenbach, S.A. Bernal, J.L. Provis, Thermodynamic modelling of alkali-activated slag cements, Appl. Geochemistry. 61 (2015) 233–247.
[44] M. James, R.J. Hunter, R.W. O'Brien, Effect of Particle Size Distribution and Aggregation on Electroacoustic Measurements of ζ Potential, Langmuir. 8 (1992) 420–423.
[45] R.F. Giese, W. Wu, C.J. Van Oss, Surface and electrokinetic properties of clays and other mineral particles, untreated and treated with organic or inorganic cations, J. Dispers. Sci. Technol. 17 (1996) 527–547.
[46] S.V. Churakov, C. Labbez, L. Pegado, M. Sulpizi, Intrinsic acidity of surface sites in calcium silicate hydrates and its implication to their electrokinetic properties, J. Phys. Chem. C. 118 (2014) 11752–11762.
[47] T. Thoenen, D. Kulik, Nagra/PSI Chemical Thermodynamic Data Base 01/01 for the GEM-Selektor (V.2-PSI) Geochemical Modeling Code: Release 28-02-03, Intern. Rep. TM-44-03-04. (2003) 1–43.
[48] C.S. Walker, S. Sutou, C. Oda, M. Mihara, A. Honda, Calcium silicate hydrate (C-S-H) gel solubility data and a discrete solid phase model at 25 °C based on two binary non-ideal solid solutions, Cem. Concr. Res. 79 (2016) 1–30.
[49] D.E. Macphee, K. Luke, F.P. Glasser, E.E. Lachowski, Solubility and aging of calcium silicate hydrates in alkaline solutions at 25 °C." Journal of the American Ceramic Society, J. Am. Ceram. Soc. 54 (1989) 646–654.
[50] G.L. Kalousek, Studies of portions of the quaternary system soda-lime-silica-water at 25 degrees C, J. Res. Natl. Bur. Stand. 32 (2012) (1934) 285.
[51] R.J. Myers, E. L'Hôpital, J.L. Provis, B. Lothenbach, Composition-solubility-structure relationships in calcium (alkali) aluminosilicate hydrate (C-(N, K-)A-S-H), Dalt. Trans. 44 (2015) 13530–13544.